Structural Engineering and Mechanics, Vol. 3, No. 5 (1995) 463-474
DOI: http://dx.doi.org/10.12989/sem.1995.3.5.463

On the large plastic deformation of tubular beams under impact loading

B. Wang†

School of Mechanical and Production Engineering, Nanyang Technological University, Singapore 2263

Abstract. When a tubular cantilever beam is loaded by a dynamic force applied transversely at its tip, the strain hardening of the material tends to increase the load carrying capacity and local buckling and cross-sectional overlization occurring in the tube section tends to reduce the moment carrying capacity and results in structural softening. A theoretical model is presented in this paper to analyze the deformation of a tubular beam in a dynamic response mode. Based on a large deflection analysis, the hardening/softening M-κ relationship is introduced. The main interest is on the curvature development history and the deformed configuration of the beam.

Key words: elastoplastic deformation; dynamic plasticity; large deflection; hardening/softening moment-curvature relationship; impact; pipe whip

1. Introduction

The response of structures under intense dynamic loading is of practical interest in many engineering areas, such as crashworthiness, collision protection, etc. The structures usually undergo large inelastic deformation under large impact loads and this poses significant problems in theoretical investigations. Due to the complexity caused by the combination of elastic and plastic deformations with moving boundaries between these two regions, only few cases are available for complete solutions. In most cases, the influence of material elasticity is usually neglected under the assumption that the input energy is many times larger than the maximum elastic energy which can be stored in the structures, also the strain hardening and strain rate effects are neglected, thus the material can be regarded as rigid-perfectly plastic and all plastic deformation can be confined at one or several individual plastic hinges. The hinge(s) may be stationary or traveling along the structural segments with the rest of the structure remains undeformed but acquires kinetic energy and moves rigidly. This idealization often allows the development of simple theoretical solutions which are satisfied for design purposes (Parkes 1955, Jones 1989, Stronge and Yu 1993, Reid, *et al.* 1995a, etc.).

For a tubular beam under transverse or bending loads, the ovalization of the cross-section reduces the bending rigidity of the tube, so that when this reduction overwhelms the effect of strain hardening of the material, the bending moment decreases from its limit-point maximum. As far as the moment-carrying capacity is concerned, a tubular beam may display hardening and softening behavior. Much work has been carried out in an effort to understand this phenomenon under static pure bending (e.g. four-point bending) conditions and on fully clamped cantilever tubes, such as Reddy (1979), Calladine (1983), Kyriakides and Ju (1992) and Yu, *et al.* (1993).

† Lecturer

However few analyses have been seen on the dynamic response of tubes. This paper, based on a rigid-plastic beam/elastic-plastic root spring model, presents an analysis on a tubular beam with a hardening/softening M-κ relationship under a step load applied transversely at its tip.

2. Theoretical modeling

With energy consideration in mind, it is assumed that the structural model consists of a rigid-perfectly plastic cantilever beam and an elastic-plastic rotational spring at the beam root (Fig.1). In other words, the beam itself has no capacity to store any elastic strain energy, but the root constraint is elastic-perfectly plastic, instead of the usual fully clamped one. This beam-spring model was first introduced by Wang and Yu (1991) in connection with the Parkes' problem (1955), an impulsively (*initial velocity*) loaded rigid-plastic cantilever beam carrying a tip mass. It was aimed to investigate the influence of material elasticity and the results showed several possible modes of response, in contrast to Parkes' single solution. The multi-mode solution agrees well with a finite element study carried out earlier by Reid and Gui (1987). This model was extended by Wang (1994) to a concentrated *dynamic force* loading resulting in several response modes with a plastic hinge initiated at a location in the beam a distance from the loading point, which is different from a *velocity* input where the hinge is inevitably started at the point of impact.

The present study is composed of two parts. First the above small deflection beam-spring model, which is only valid at initial stages of the impact, is extended to a large deflection one, thus the deformation history and configurations of the deformed beam can be examined. Secondly, a rigid, hardening/softening model is applied to the beam in which a plastic zone (not a hinge any more) is formed. With the plastic zone traveling (in a similar way to a traveling hinge) towards the root of the beam, permanent curvature along the tube is formed. An iterative algorithm is developed to calculate the exact solution.

2.1. Governing equations of the beam-spring model

Consider a straight beam subjected to a dynamic force F applied at its tip, it is assumed that there is an elastic-perfectly plastic rotational spring at the root of the beam, as shown in Fig.1. The beam is made from a rigid-perfectly plastic material and has mass per unit length μ, total length L and a tip mass G. The spring becomes plastic when the moment on it reaches M_0 (see Fig. 2), exactly the same value of the dynamic fully plastic bending moment at the cross-section of the beam. The elastic stiffness K is defined on the basis that all of the elastic strain energy capacity of the beam is lumped into the root spring. Thus while the beam is considered to be rigid, the system as a whole has the same elastic energy storage capacity as that of a fixed-ended elastic plastic beam, which means $K=EI/L$, where EI is the flexural rigidity

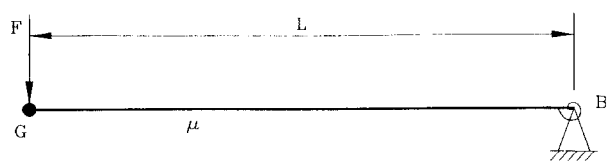

Fig. 1 The beam-spring model.

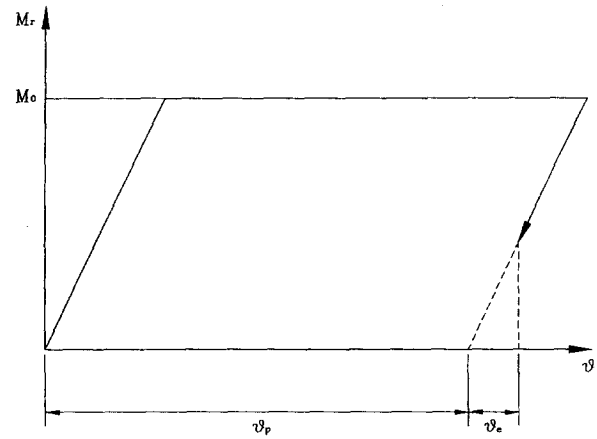

Fig. 2 Characteristics of the rotational spring at the beam root.

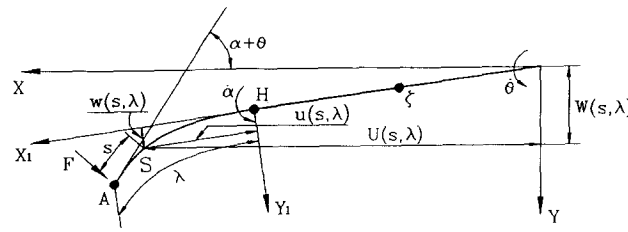

(a) Coordinates and angular velocites for large deflection analysis

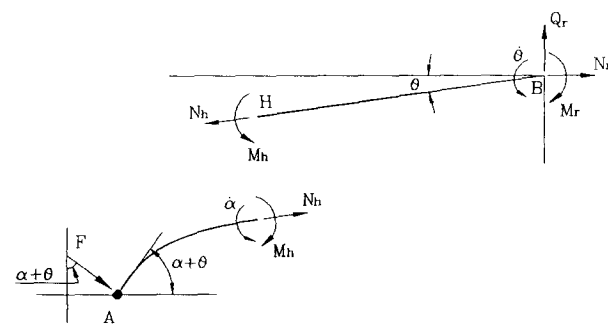

(b) Bending moments and forces at ends of beam segments

Fig. 3 Definitions of coordinates and free body diagram.

of the beam as if its elastic properties were not ignored.

Static analysis shows that when $F \leq F_0 = M_0/L$, there will be no failure anywhere. And when $F > F_0$, a plastic hinge will appear either at root B or in the beam.

Assuming that a hinge H is formed at a distance λ from the tip in the cantilever, Fig. 3 shows the coordinates and free-body diagram of beam segments. $\dot{\vartheta}$ is the angular velocity of the rotational spring at the root, $\dot{\alpha}$ is the angular velocity of segment AH at the hinge relative to segment HB. Derivation of the governing equations of the beam is given in an appendix and they are listed as follows.

For segment AH

$$G\ddot{U}(0,\ \lambda)+\mu\int_0^{\lambda}\ddot{U}(s,\ \lambda)ds=-(F\sin(\vartheta+\alpha)+N_h\cos\vartheta) \tag{1}$$

$$G\ddot{W}(0,\ \lambda)+\mu\int_0^{\lambda}\ddot{W}(s,\ \lambda)ds=F\cos(\vartheta+\alpha)+N_h\sin\vartheta \tag{2}$$

where N_h is the axial force at the hinge caused in part by the centrifugal effect of the angular velocity in segment AH. Since it does not produce any bending moment about the root B, the rate of change of moment of momentum of segment AH about B is

$$G[U(0,\ \lambda)\ddot{W}(0,\ \lambda)-W(0,\ \lambda)\ddot{U}(0,\ \lambda)]+\mu\int_0^{\lambda}[U(s,\ \lambda)\ddot{W}(s,\ \lambda)-W(s,\ \lambda)\ddot{U}(s,\ \lambda)]ds$$
$$=F\cos(\theta+\alpha)U(0,\ \lambda)+F\cos(\theta+\alpha)W(0,\ \lambda)-M_h \tag{3}$$

M_h being the bending moment at the hinge.

For segment HB, it gives

$$\mu\int_{\lambda}^{L}\ddot{U}(s)ds=N_h\cos\vartheta-N_r \tag{4}$$

$$\mu\int_{\lambda}^{L}\ddot{W}(s)ds=N_h\sin\vartheta-Q_r \tag{5}$$

$$\mu\int_{\lambda}^{L}[U(s)\ddot{W}(s)-W(s)\ddot{U}(s)]ds=M_h-M_r \tag{6}$$

where Q_r and M_r are the shear force and moment at the beam root, respectively. Explicit expressions of the above governing equations are given in an appendix.

The yield criterion at the hinge are

$$\left|\frac{M_h}{M_0}\right|+\left(\frac{N_h}{N_0}\right)^2=1 \tag{7}$$

Note that at $t=0$, N_h, $M_h(=K\vartheta)$ and all angular velocities are zero, and also $M_h=M_0$. After a lengthy manipulation, we have

$$F=\left(GL+\mu\lambda_0\left(L-\frac{\lambda_0}{2}\right)\right)\frac{3M_0}{\mu(L-\lambda_0)^3}+\left(G+\frac{\mu}{2}\right)\frac{3M_0}{\mu\lambda_0^2}\left(1-\left(\frac{3L}{2}-\lambda_0\right)\frac{\lambda_0^2}{(L-\lambda_0)^3}\right) \tag{8}$$

Thus, with the magnitude of the dynamic force F given, the initial hinge position can be calculated from Eq. (8). The moment at the beam root is given by its definition:

$$M_r=\begin{cases}K\vartheta_e & \text{elastic or unloading}\\ \pm M_0 & \text{otherwise}\end{cases} \tag{9}$$

There are in total seven unknowns in the above Eqs. (1) to (7) and they can be solved with a standard numerical procedure, such as a fourth order Runge-Kutta method.

2.2. A hardening/softening model

The hardening/softening M-κ (bending moment-curvature) relationship of a tube can be determined experimentally or numerically, provided the stress-strain relation of the material and dimensions of the tubular cross-section are specified. Assuming that the tube material obey a

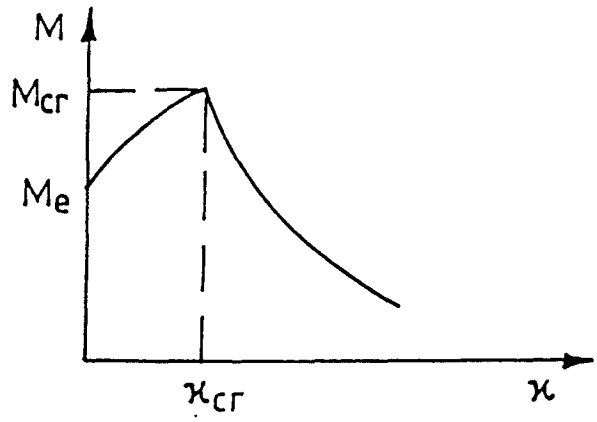

Fig. 4 Idealized bending moment-curvature relationship.

power law relationship between stress, σ, and plastic strain, ε_p, this serves as a good representation for the mild and stainless steel. Then the critical curvature κ_{cr}, at which the bending moment attains a maximum, is estimated as

$$\kappa_{cr} \approx \frac{0.7t\sqrt{n}}{a^2} \tag{10}$$

where t and a are the wall thickness and the average radius of the tube, respectively, and n is the index in the power law $\sigma = A\varepsilon_p^n$. By taking the material strain-hardening and the ovalisation of the cross-sections into account, a three-phase M-κ relationship is obtained: (i) rigid phase, $M < M_e$, $\kappa = 0$; (ii) hardening phase, $M_e \leq M \leq M_{cr}$, $0 < \kappa \leq \kappa_{cr}$; (iii) softening phase, $M \leq M_{cr}$, $\kappa_{cr} < \kappa$, as shown in Fig. 4. The above rigid-perfectly plastic model can be modified to incorporate this M-κ relationship. Computation of the dynamic deformation of a tube can be carried out in the following steps:

Step 1. At each time instant t, assume a value of M_p, where $M_e \leq M_p \leq M_s$, M_e and M_s being respectively the elastic bending moment limit of the tube and the maximum value of bending moment at which softening starts in the hardening/softening model. By using M_p as M_0, Eqs. (1) to (7) can be solved and the bending moment distribution along the tube can be obtained.

Step 2. Calculate curvature distribution in the plastic zone where the bending moment is higher than M_e by using the hardening/softening M-κ relationship.

Step 3. Calculate angular acceleration distribution in the plastic zone, then from which, shear force distribution in the beam.

Step 4. Calculate bending moment distribution along the beam and compare with the original bending moment distribution in Step 1.

Step 5. Iterate the whole procedure by changing the value of M_p until an accepted accuracy of an "accurate" bending moment distribution is obtained. Then the shear force and curvature distribution can be settled.

Step 6. Repeat Steps 1 to 5 for the next time interval, $t + \delta t$ until the hinge reaches the root or ceases to act.

Step 2 can be performed by discretising the plastic region into small segments, as shown in Fig. 5, then through pre-defined M-κ relationship one can get rotational angles then angular accelerations over each individual segment. Since the material is assumed rigid-hardening/softening, there is no spring-back. Thus as long as the maximum bending moment during the

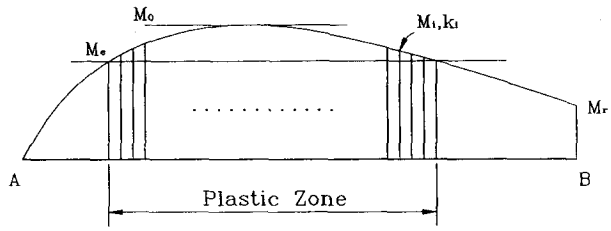

Fig. 5 Distribution of plastic zone.

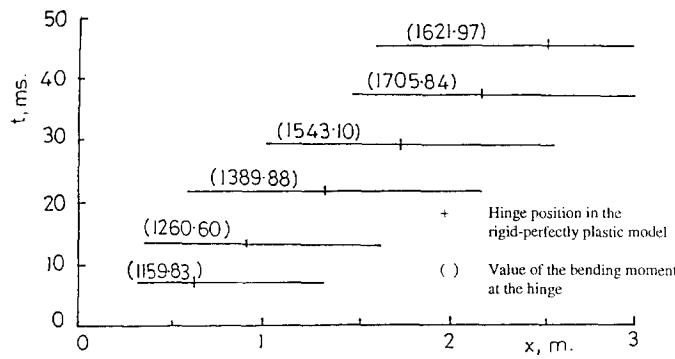

Fig. 6 Development of plastic zone. Step loading, $F=17000$ N.

entire response for every cross-section is recorded, the final curvature distribution can be determined.

3. Numerical results

Calculations were carried out on a two inch bore mild steel specimen. It has an outside diameter of 50.8 mm, a wall thickness of 2.6 mm, a total length of 3 m and a mass per unit length of 3.22 kg/m. The tip mass is 1.8 kg on which a step force was applied transversely. For this tube, M-κ relationship is approximated by

(i) in the rigid phase

$$\kappa=0,\ M<M_e=\frac{3\pi}{16}M_p=1050\ \text{Nm};$$

(ii) in the hardening phase

$$M(\kappa)=1050+920\kappa-300\kappa^2,\ 0\leq\kappa\leq\kappa_{cr}$$

(iii) in the softening phase

$$M(\kappa)=1900(1-0.031\,\kappa^2),\ \kappa>\kappa_{cr}$$

Different load magnitudes were used to examine the effect of the amount of externally supplied energy on the response of the tube. For a step loading of magnitude $F=17{,}000$N, Fig. 6 shows the plastic region formed along the pipe at various time, which is clearly different from the

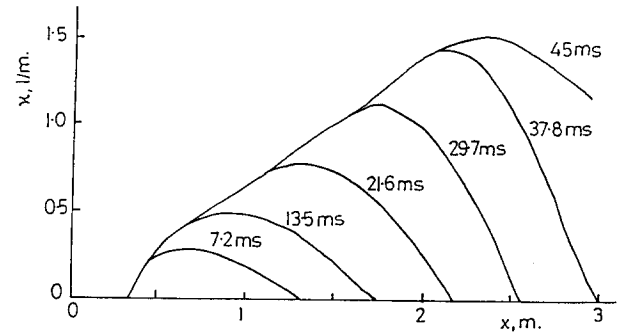

Fig. 7 Curvature evolution along the tube. Step loading, $F=17000$ N.

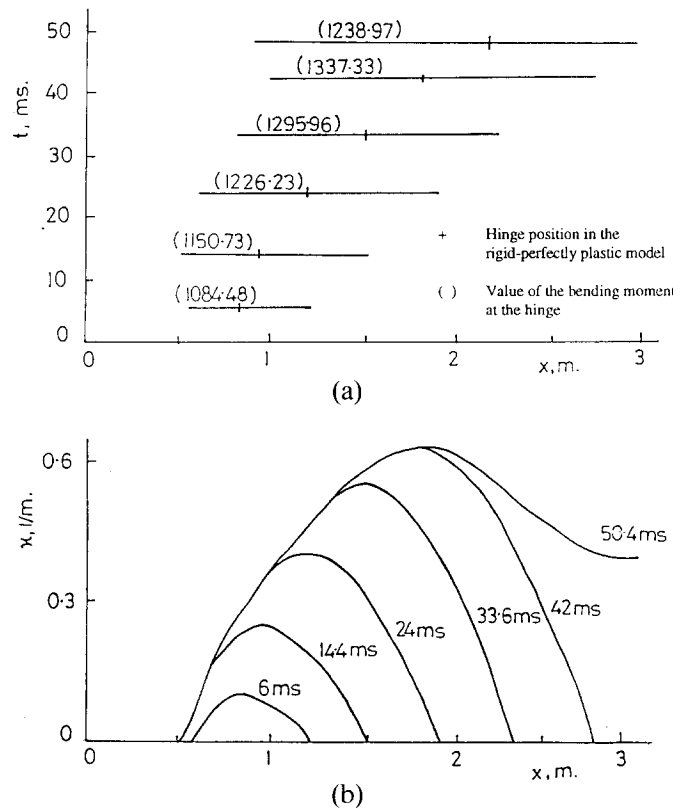

Fig. 8 (a) Development of plastic zone. Step loading, $F=8000$ N;
(b) Curvature evolution along the beam. Step loading, $F=8000$ N.

plastic hinge in a rigid-perfectly plastic model as discussed by Reid and Wang (1995b). Note that the energy is dissipated in all the plastic zone in this model while in the rigid-perfectly plastic one, only the hinge consumes energy. The plastic region expands while it moves towards the root of the tube, and the boundaries of the plastic region indicate the loading and unloading fronts in the pipe. Curvature develops along the tube as the plastic region moves. Fig.7 gives the curvature distribution history of the pipe under the same load. Clearly, the value of curvature

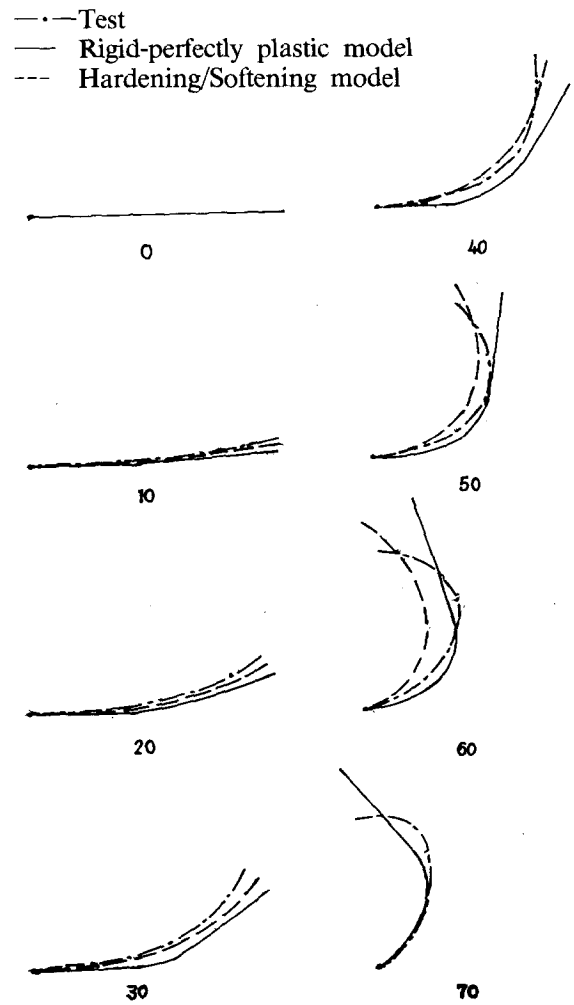

Fig. 9 Comparison of deformed tube on hardening/softening, rigid, perfectly plastic models and test results (Reid, *et al.* 1995a)

increases while the deformation progresses. According to the rigid-perfectly plastic model, the beam root is not disturbed until the traveling hinge reaches there and makes a transition for the dynamic response from a transient phase to a model phase. In the present hardening/softening model, however, the root begins its plastic deformation much earlier, and sustains more plastic deformation when the peak of bending moment approaches it.

Fig. 8 shows another example. The step load is $F=8{,}500$ N, beam parameters being the same. Compared with the above case, the loading is much less and so is the curvature. Fig. 9 gives the comparison amongst the deformed beam configurations based on the hardening/softening model, the rigid-perfectly plastic model and experimental results (Reid and Wang 1995b) under the same load magnitude. The improvement of the deformed beam shape under the hardening/softening model is clearly illustrated.

4. Discussions

Based on a large deflection, rigid-perfect plastic model, an analysis on the hardening/softening characteristics of a tubular beam under a transversely applied dynamic load has been performed. The elasticity of the beam is lumped to a rotational spring at its root. It shows that the curvature distribution along the tube due to its dynamic plastic deformation can be calculated through iteration of bending moment distribution thus an exact solution was achieved. The nature of the large deflection analysis makes it possible to compare the deformed configurations of a dynamically deforming tube with those of tested specimens. Improvements in the deformed shapes are clearly demonstrated.

In the present model, the beam root remains elastic-perfectly plastic. Yu, *et al.* (1993) studied the deformation of the end portion of a fully clamped tubular cantilever under a tip force loading. Incorporation of their finding may further improve the current hardening/softening model.

Acknowledgements

The author sincerely acknowledges Professor T.X. Yu for his encouragement and guidance throughout this work.

References

Calladine, C.R. (1983), *Plastic buckling of tubes in pure bending,* Collapse: the Buckling of Structures in Theory and Practice (ed. by Thompson, J.M.T. and Hunt, G.W.), Cambridge, 111-124.

Jones, N. (1989), *Structural impact,* Cambridge University Press.

Kyriakides, S. and Ju, G.T. (1992), "Bifurcation and localization instabilities in cylindrical shell under bending-I. Experiments", *Int. J. Solids Structures,* **29**, 1117-1142.

Parkes, E.W. (1955), "The permanent deformation of a cantilever struck transversely at its tip", *Proc. Royal Society, Series A,* **228**, 482-476.

Reddy, B.D. (1979), "Plastic buckling of a cylindrical shell in pure bending", *Int. J. Mech. Sci.,* **21**, 671-679.

Reid, S.R. and Gui, X. (1987), "On the elastic-plastic deformation of cantilever beams subjected to tip impact", *Int. J. Impact Engng.,* **2**, 109-127.

Reid, S.R., Wang, B. and Yu, T.X. (1995a), "Yield mechanisms of a bent cantilever beam subjected to a suddenly applied constant out-of-plane tip force", *Int. J. Impact Engng.,* **16**, 49-73.

Reid, S.R. and Wang, B. (1995b), "Large deflection analysis of whipping pipes-Part I: Rigid-perfectly plastic model", *ASCE Journal of Engineering Mechanics,* in press.

Strong, W.J. and Yu, T.X. (1993), *Dynamic models for structural plasticity*, Springer-Verlag.

Yu, T.X., Reid, S.R. and Wang, B. (1993), "Hardening-softening behavior of tubular cantilever beams", *Int. J. Mech. Sci.,* **35**, 1021-1033.

Wang, X. and Yu, T.X. (1991), "Parkes revised: when elastic deformation at the root of a cantilever beam is involved", *Int. J. Impact Engng.,* **11**, 197-209.

Wang, B. (1994), "Failure mechanisms of a rigid-perfectly plastic cantilever with elastic deformation at its root subjected to tip pulse loading", *Structural Engineering and Mechanics,* **2**(2), 141-156.

Appendix

Derivation of governing equations of the beam-spring model

Assuming that under the dynamic tip load, a plastic hinge H is formed at a location in the beam measured λ from the tip. Fig. 3 shows the definition of the coordinates. System XBY is fixed at B with X in the undeformed direction of BA and system X_1HY_1 has its origin at the current hinge H with X_1 in the direction of the rigid segment BH. With the hinge moving towards B and segment HB rotating about the root, system X_1HY_1 is a local moving frame. And frame XBY can be regarded as a global static one. Denote ϑ the angular rotation of the rotational spring at the root, and α the angular rotation of segment AH at the hinge relative to segment HB. For an arbitrary point S in segment AH, its coordinates in system X_1HY_1 are

$$u(s,\ \lambda)=\int_0^{\lambda}\cos\alpha(\xi,\ \lambda)d\xi \tag{A1}$$

and

$$w(s,\ \lambda)=\int_0^{\lambda}\sin\alpha(\xi,\ \lambda)d\xi \tag{A2}$$

In global system XBY, they become

$$U(s,\ \lambda)=U_h+u(s,\ \lambda)\cos\vartheta-w(s,\ \lambda)\sin\vartheta \tag{A3}$$

$$W(s,\ \lambda)=W_h+u(s,\ \lambda)\sin\vartheta+w(s,\ \lambda)\cos\vartheta \tag{A4}$$

where U_h and W_h are coordinates of hinge H in system XBY which are obtained by putting $\zeta=\lambda$ in the following coordinates of an arbitrary point, distance ζ from A in segment HB in global XBY system,

$$U(\zeta)=(L-\zeta)\cos\vartheta \tag{A5}$$

$$W(\zeta)=(L-\zeta)\sin\vartheta \tag{A6}$$

ζ being within the region $[\lambda,\ L]$ and L being the total length of the beam. Thus coordinates of point S can be written as

$$U(s,\ \lambda)=[L-\lambda+u(s,\ \lambda)]\cos\vartheta-w(s,\ \lambda)\sin\vartheta \tag{A7}$$

$$W(s,\ \lambda)=[L-\lambda+u(s,\ \lambda)]\sin\vartheta-w(s,\ \lambda)\cos\vartheta \tag{A8}$$

Differentiating Eqs. (A5) to (A8) twice with respect of time produces the corresponding accelerations,

$$\ddot{U}(\zeta)=-(L-\zeta)\sin\vartheta\ddot{\vartheta}-(L-\zeta)\cos\vartheta\dot{\vartheta}^2 \tag{A9}$$

$$\ddot{W}(\zeta)=(L-\zeta)\cos\vartheta\ddot{\vartheta}-(L-\zeta)\sin\vartheta\dot{\vartheta}^2 \tag{A10}$$

$$\begin{aligned}\ddot{U}(s,\ \lambda)=&-[(L-\lambda)\sin\vartheta+u(s,\ \lambda)\sin\vartheta+w(s,\ \lambda)\cos\vartheta]\ddot{\vartheta}\\&-[(u(s,\ \lambda)\sin\vartheta+w(s,\ \lambda)\cos\vartheta]\ddot{\alpha}\\&-[(L-\lambda)\cos\vartheta+u(s,\ \lambda)\cos\vartheta-w(s,\ \lambda)\sin\vartheta]\dot{\vartheta}^2\\&-[u(s,\ \lambda)\cos\vartheta-w(s,\ \lambda)\sin\vartheta]\dot{\alpha}^2\\&-2[(u(s,\ \lambda)\cos\vartheta-w(s,\ \lambda)\sin\vartheta]\dot{\vartheta}\dot{\alpha}-\sin\vartheta\dot{\lambda}\dot{\alpha}\end{aligned} \tag{A11}$$

$$\begin{aligned}\ddot{W}(s,\ \lambda)=&[(L-\lambda)\cos\vartheta+u(s,\ \lambda)\cos\vartheta-w(s,\ \lambda)\sin\vartheta]\ddot{\vartheta}\\&+[u(s,\ \lambda)\cos\vartheta-w(s,\ \lambda)\sin\vartheta]\ddot{\alpha}\\&-[(L-\lambda)\sin\vartheta+u(s,\ \lambda)\sin\vartheta+w(s,\ \lambda)\cos\vartheta]\dot{\vartheta}^2\\&-[u(s,\ \lambda)\sin\vartheta+w(s,\ \lambda)\cos\vartheta]\dot{\alpha}^2\\&-2[u(s,\ \lambda)\sin\vartheta+w(s,\ \lambda)\cos\vartheta]\dot{\vartheta}\dot{\alpha}+\cos\vartheta\dot{\lambda}\dot{\alpha}\end{aligned} \tag{A12}$$

Substituting the above accelerations into Eqs. (1) to (6) gives the explicit form of the governing equations.

For segment AH, the equation of translational motion in X direction is

$$\begin{aligned}
&\{G[(L-\lambda)\sin\vartheta+u(0,\ \lambda)\sin\vartheta+w(0,\ \lambda)\cos\vartheta]\\
&+\mu[(L-\lambda)\lambda\sin\vartheta+i_1(\lambda)\sin\vartheta+i_2(\lambda)\cos\vartheta]\}\ddot{\vartheta}\\
&+\{G[u(0,\ \lambda)\sin\vartheta+w(0,\ \lambda)\cos\vartheta]+\mu[i_1(\lambda)\sin\vartheta+i_2(\lambda)\cos\vartheta]\}\ddot{\alpha}\\
&+\{G[(L-\lambda)\cos\vartheta+u(0,\ \lambda)\cos\vartheta-w(0,\ \lambda)\sin\vartheta]\\
&+\mu[(L-\lambda)\lambda\cos\vartheta+i_1(\lambda)\cos\vartheta-i_2(\lambda)\sin\vartheta]\}\dot{\vartheta}^2\\
&+\{G[u(0,\ \lambda)\cos\vartheta-w(0,\ \lambda)\sin\vartheta]+\mu[i_1(\lambda)\cos\vartheta-i_2(\lambda)\sin\vartheta]\}\dot{\alpha}^2\\
&+2\{G[u(0,\ \lambda)\cos\vartheta-w(0,\ \lambda)\sin\vartheta]+\mu[i_1(\lambda)\cos\vartheta-i_2(\lambda)\sin\vartheta]\}\dot{\vartheta}\dot{\alpha}\\
&+(G+\mu\lambda)\sin\vartheta\dot{\alpha}\dot{\lambda}\\
&=F\sin(\vartheta+\alpha)+N_h\cos\vartheta
\end{aligned}\tag{A13}$$

where $i_1=\int_0^\lambda u(s,\ \lambda)ds$ and $i_2=\int_0^\lambda w(s,\ \lambda)ds$ are the first moments of the deformed segment about the local frame X_1HY_1.

The equation of translational motion in Y direction is

$$\begin{aligned}
&\{G[(L-\lambda)\cos\vartheta+u(0,\ \lambda)\cos\vartheta-w(0,\ \lambda)\sin\vartheta]\\
&+\mu[(L-\lambda)\lambda\cos\vartheta+i_1(\lambda)\cos\vartheta-i_2(\lambda)\sin\vartheta]\}\ddot{\vartheta}\\
&+\{G[u(0,\ \lambda)\cos\vartheta-w(0,\ \lambda)\sin\vartheta]+\mu[i_1(\lambda)\cos\vartheta-i_2(\lambda)\sin\vartheta]\}\ddot{\alpha}\\
&-\{G[(L-\lambda)\sin\vartheta+u(0,\ \lambda)\sin\vartheta+w(0,\ \lambda)\cos\vartheta]\\
&+\mu[(L-\lambda)\lambda\sin\vartheta+i_1(\lambda)\sin\vartheta+i_2(\lambda)\cos\vartheta]\}\dot{\vartheta}^2\\
&-\{G[u(0,\ \lambda)\sin\vartheta+w(0,\ \lambda)\cos\vartheta]+\mu[i_1(\lambda)\sin\vartheta+i_2(\lambda)\cos\vartheta]\}\dot{\alpha}^2\\
&-2\{G[u(0,\ \lambda)\sin\vartheta+w(0,\ \lambda)\cos\vartheta]+\mu[i_1(\lambda)\sin\vartheta+i_2(\lambda)\cos\vartheta]\}\dot{\vartheta}\dot{\alpha}\\
&+(G+\mu\lambda)\sin\vartheta\dot{\alpha}\dot{\lambda}\\
&=F\cos(\vartheta+\alpha)+N_h\sin\vartheta
\end{aligned}\tag{A14}$$

The rotational equation of AH about B is

$$\begin{aligned}
&\{G[(L-\lambda)^2+u^2(0,\ \lambda)+w^2(0,\ \lambda)+2(L-\lambda)u(0,\ \lambda)]\\
&+\mu[(L-\lambda)^2\lambda+i_0(\lambda)+2(L-\lambda)i_1]\}\ddot{\vartheta}\\
&+\{G[(L-\lambda)u(0,\ \lambda)+u^2(0,\ \lambda)+w^2(0,\ \lambda)]+\mu[i_0(\lambda)+2(L-\lambda)i_1]\}\ddot{\alpha}\\
&-[G(L-\lambda)w(0,\ \lambda)+\mu(L-\lambda)i_2]\dot{\alpha}^2-2[G(L-\lambda)w(0,\ \lambda)+\mu(L-\lambda)i_2]\dot{\vartheta}\dot{\alpha}\\
&\{G[(L-\lambda+u(0,\ \lambda)]+\mu[(L-\lambda)\lambda+i_1]\}\dot{\alpha}\dot{\lambda}\\
&=F[L-\lambda+u(0,\ \lambda)]\cos\alpha+Fw(0,\ \lambda)\sin\alpha-M_h
\end{aligned}\tag{A15}$$

where $i_0=\int_0^\lambda[u^2(s,\ \lambda)+w^2(s,\ \lambda)]ds$ is the second moment of the deformed segment about the current hinge.

For segment HB, the equations of translational motion in X and Y directions are, respectively,

$$\frac{\mu}{2}(L-\lambda)^2\sin\vartheta\ddot{\vartheta}+\frac{\mu}{2}(L-\lambda)^2\cos\vartheta\dot{\vartheta}^2=N_r-N_h\cos\vartheta\tag{A16}$$

and

$$\frac{\mu}{2}(L-\lambda)^2\cos\vartheta\ddot{\vartheta}-\frac{\mu}{2}(L-\lambda)^2\sin\vartheta\dot{\vartheta}^2=-Q_r+N_h\cos\vartheta \tag{A17}$$

The equation of rotational motion about B is

$$\frac{\mu}{3}(L-\lambda)^3=M_h-M_r. \tag{A18}$$

There are in total seven unknowns, i.e., λ, ϑ, α, M_h, N_h, N_r, Q_r. Combined with Eqs. (7) and (9), Eqs. (A13) to (A18) can be solved numerically.

Let the root rotation be zero, then $\ddot{\vartheta}=\dot{\vartheta}=\vartheta=0$. This is equivalent to a fully clamped beam. Then Eqs. (A13) to (A15) become identical to the governing equations in a large deflection, rigid-perfectly plastic analysis of a straight cantilever, as discussed by Reid, *et al.* (1995a).